Quantum well infrared optoelectronic devices

F. F. SIZOV

Institute of Semiconductors of the Academy of Sciences of the Ukraine,
pr. Nauki 45, 252650 Kiev, Ukraine

A. ROGALSKI

Institute of Technical Physics, WAT,
00-908 Warsaw, Poland

1. Introduction

At present $Hg_{1-x}Cd_xTe$ (HgCdTe) is the most important intrinsic semiconductor alloy system for infrared detectors. However, in spite of achievements in material and device quality, difficulties still exist due to lattice, surface, and interface instabilities. This realization have intensified the search for alternative infrared materials.

In the class of alternative materials, three groups of IR detectors are developed:

a) photoemissive metal silicide Schottky barriers;
b) intrinsic detectors made from ternary alloy systems such as InAsSb, HgZnTe and HgMnTe;
c) quantum well IR detectors.

The last class of photon IR detectors has emerged from the large research activity aimed at new types of solid state material, which can be obtained by assembling multilayer structures in which two components alternate in very thin films. In the present paper the basic physical concepts and performance of the quantum well detectors are briefly reviewed.

Since the initial proposal by Esaki and Tsu [1] and advent of molecular beam epitaxy (MBE), the interest in semiconductor superlattice (SL) and quantum well (QW) structures has increased continuously over the years, driven by technological challenges, new physical concepts and phenomena as well promising applications. Here we focus on devices which involves IR excitation of carriers in quantum wells. A distinguishing feature of these devices is that they can be implemented in chemically stable wide band gap materials as a result of the used of intraband processes. On account of this it is possible to use such material systems as GaAs/AlGaAs, InGaAs/InAlAs, InAs/GaInSb, SiGe/Si, as well as other systems, although most of the experimental works have been carried out with GaAs/AlGaAs. These materials have fewer processing problems than HgCdTe, and achievement of monolithic focal plane arrays (FPAs) could also be implemented. Quantum well IR detectors with response in wavelength region from 3 μm to 15 μm have been demonstrated. Table 1 summarizes performance of different type of quantum well IR detectors. For IR semiconductor laser applications in the spectral range of 3–20 μm the basic role play QWs of IV–VI systems which are supposed to operate at elevated temperatures compare to $T = 77$ K.

There are some possible types of QW IR optoelectronic devices connected with different types (type I, type II, and type

Table 1. **Performance of quantum well infrared detectors (after Ref. [21])**

Type	Mode	λ_p [μm]	T [K]	R [A/W]	D* [cm Hz$^{1/2}$W^{-1}]
GaAs/AlGaAs	PC	8.3	77	0.42	$1.0 \cdot 10^{10}$
	PC	9.8	68	1.2	$2.0 \cdot 10^{10}$
	PC	≈ 10.0	4.2		$> 3.0 \cdot 10^{13}$
	PC	7.9	77	1.0	$4.0 \cdot 10^{10}$
	PC	13.2	77		$1.0 \cdot 10^{9}$
			60		$6.3 \cdot 10^{9}$
			50		$3.3 \cdot 10^{10}$
	PC	7.2	77	0.039	$3.1 \cdot 10^{11}$
	PV	4.2	77	0.05	$1.1 \cdot 10^{12}$
InGaAs/InAlAs	PC	4.1	77		$2.3 \cdot 10^{10}$
InGaAs/InP	PC	7.6	77	1.2	$9.0 \cdot 10^{10}$
	PC	2.7	77	0.14	$3.0 \cdot 10^{10}$
InGaAsP/InP	PC	8.6	77	0.51	$5.3 \cdot 10^{9}$
		12.1	50	0.3	$1.3 \cdot 10^{9}$
SiGe/Si	PC	8.6	77	0.3	$1.0 \cdot 10^{9}$
	PC	10.8	77	0.04	$3.3 \cdot 10^{9}$
GaAs/AlGaAs	PC, PV	8.9	77	0.38	$1.6 \cdot 10^{10}$
InAsSb/InSb	PV	≈ 10.0	77		$\approx 1.0 \cdot 10^{10}$
PbTe-*n-i-p-i*	PC	5.8	77		$8.0 \cdot 10^{10}$
		4.7	140		$5.0 \cdot 10^{10}$

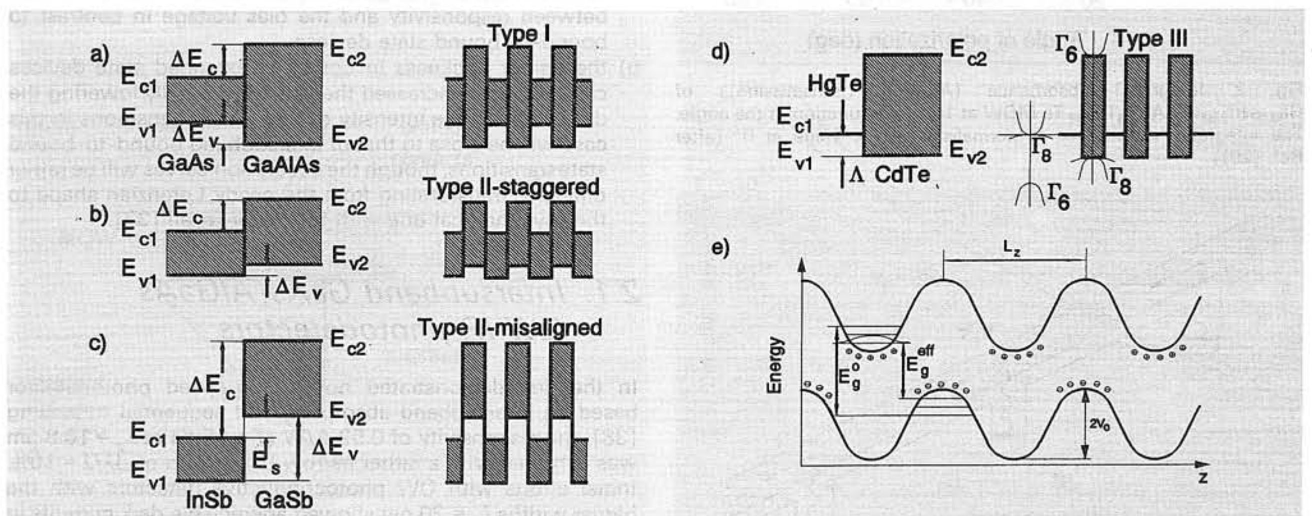

Fig. 1. Various types of semiconductor SL's and MQW's structures: (a) type I structure; (b) type II „misaligned" structure; (c) type II „staggered"structure; (d) type III structure; (e) *n-i-p-i* structure. L_z is the period of structure, $2V_0$ is the modulation potential and E_g^{eff} is the effective band gap

III) discontinuities at the heterointerface [2]. The various types of the discontinuities at the heterointerface are shown in Fig. 1. In multiple QWs (MQWs) and SLs electrical and optical properties are mostly governed by the band discontinuities at the heterointerface, of course, taking into account the semiconductor band structure.

Recently there have been considerable efforts to understand the interface phenomena and to measure the band offset at semiconductor interfaces [3–9]. For obtaining the values of the band offsets several methods have been used, which are based on optical experiments [10,11], electrical measurements of device characteristics [12,13], photoemission [14,15] and photovoltaic experiments [16]. Also inelastic light scattering [9] and electron-beam-induced current measurements [17,18] are used for this aim. It must be taken into account that electrical and optical methods do not measure the band offsets themselves, but quantities associated with the electronic structure of the heterojunction. To determine the band offset from these experiments an appropriate theoretical model is required.

Modern epitaxial techniques, such as molecular beam epitaxy and metalorganic chemical vapour deposition (MOCVD) [19] for growth III-V and II–VI compounds, and laser-induced evaporation [20,21] in application to II–VI and IV–VI semiconductors, have made it technologically possible to grow artificially layered semiconductors of high structural perfection at the interface.

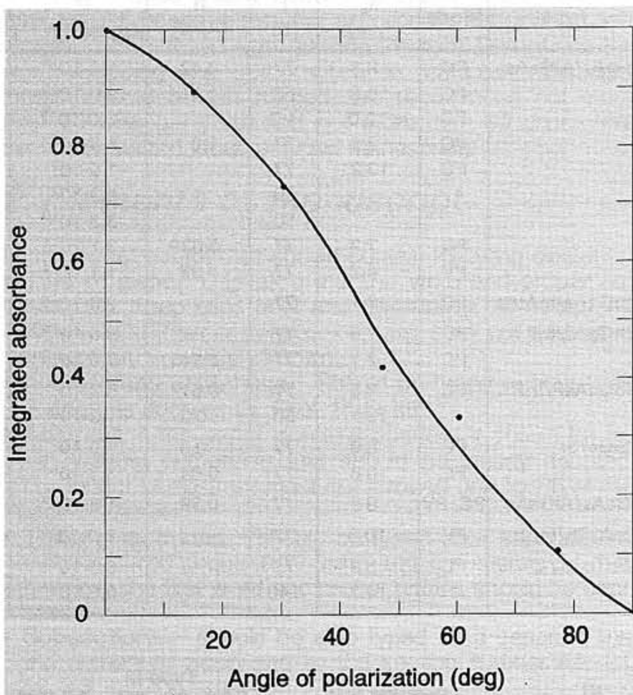

Fig. 2. Integrated absorbance (A = -log (transmission)) of $Ga_{0.47}In_{0.53}As/Al_{0.48}In_{0.52}Te$ MQW at 10 K as a function of the angle. The integrated absorbance is normalized to the value at 0° (after Ref. [20])

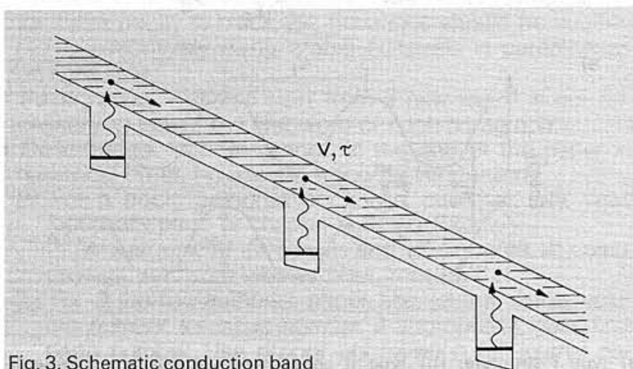

Fig. 3. Schematic conduction band diagram of the quantum well detector (after Ref. [36])

An important requirement for high-quality MQWs and SLs is the matching of the lattice constants of the constituents. But in pseudomorphic systems (so-called strained-layer SLs (SSLs)) internal mechanical strain due to lattice constants mismatch, can be used as an additional effect in bandgap engineering [22–24].

2. Intersubband (intraband) QW IR photodetectors

In bulk semiconductors the intraband dipole optical transitions are forbidden and may only be induced by phonons or impurities. In QWs and SLs the intersubband (intraband) transitions are allowed between the envelope states and the Bloch states remain constant. This situation differs the interband valence-to conduction band optical dipole transitions which occur between the Bloch states. Moreover, the intersubband transitions are only possible for the component of the electric field perpendicular to the QW or SL plane [25]. The dependence of integrated absorbance as a function of angle between the electromagnetic field vector and the SL axis is shown in Fig. 2. Still, large dipole matrix elements for intersubband optical transitions are only a few times less then for interband dipole optical transitions. That determines large intersubband optical absorption, which will be delta-like due to congruent in-plane dispersion relations of the initial and final subbands. Non-parabolicity, the wells's and walls's width non-conservation and other effects, the final values of relaxation times of the excited states would change the delta peak into a spectral line of final width.

In 1987, Levine and co-workers [27] fabricated the first quantum well infrared detector operating at 10 μm. This detector design was based on a transition between two confined states in the quantum well by an applied field. The intersubband absorption was studied in GaAs/AlGaAs [27–29], InGaAs/InAlAs [30,31], InGaAs/AlGaAs [32], InGaAs/InP [33] SiGe/Si [34,35] MQWs and SLs. However, the bound-to-bound transitions are not useful for detection, since photoexcited carriers may not readily escape from excited bound states. Recently, considerable attention was paid to "bound-to-extended" state absorption MQW detectors [36]. In such photodetectors the electrons are excited by IR radiation (polarized as in the case of intersubband photodetectors) from the ground symmetrical state in the well to an antisymmetrical extended state pushed slightly out of the well. These are schematically shown in Fig. 3.

The rapid progress in this direction is caused by following conditions:

a) bound-to-extended state devices require much less biases to observe a photosignal and there exist a linear relation between responsivity and the bias voltage in contrast to bound-to-bound state devices;
b) the barrier thickness in bound-to-extended state devices can be greatly increased thereby substantially lowering the dark current. The intensity of the optical transitions in this case will be close to that of intersubband bound-to-bound state transitions, though the absorption curves will be rather different, transforming from the nearly Lorenzian shape to the asymmetrical one with high energy tail [37].

2.1. Intersubband GaAs/AlGaAs QW IR photodetectors

In the first demonstrated novel high-speed photodetector based on intersubband absorption and sequential tunnelling [38], the responsivity of 0.52 A/W (T = 15 K) at λ_p = 10.8 μm was achieved with a rather narrow bandwidth of $\Delta\lambda/\lambda$ = 10%. Initial efforts with QW photoconductive detectors with the barrier widths L_b = 20 nm showed appreciable dark currents in which are involved three relevant mechanisms: tunnelling, phonon assisted tunnelling and thermionic emission out of QWs. Tunnelling is the dominant dark current mechanism in the

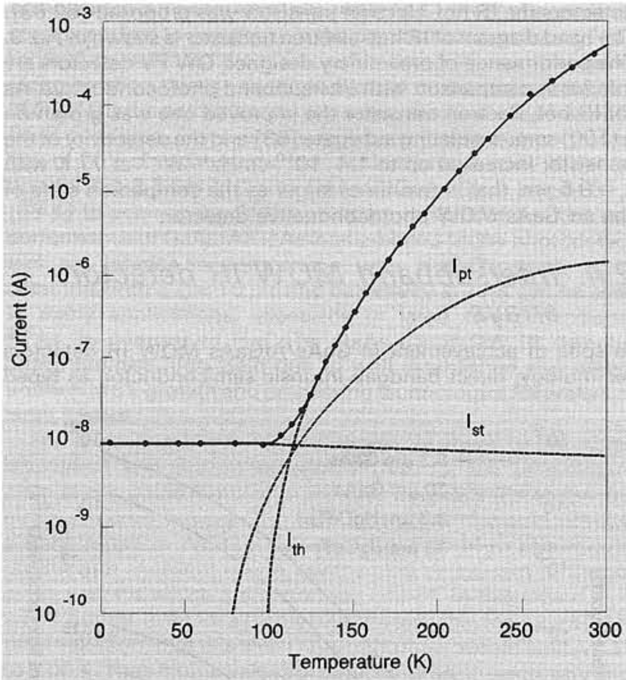

Fig. 4. Temperature dependence of the dark current at low bias for bound-to-bound multiple GaAs/$Al_{0.36}Ga_{0.64}As$ device (50 periods with 7 nm wells and 14 nm barriers). The subscripts "th", "st" and "pt" refer to thermonic, tunneling and photon-assisted tunneling mechanisms, respectively (after Ref. [39])

low temperature region, while thermionic emission limits the performance at high operating temperatures. Thermionic emission generally limits 10 μm photoconductive type MQW detectors to operating temperatures less than about 70 K [39,40]. Temperature dependence of the dark current for GaAs/AlGaAs MQW device is shown in Fig. 4.

By increasing the barrier width up to $L_b = 50$ nm, the tunnelling of GaAs/AlGaAs QW is reduced by more than one order of magnitude and the responsivity is highly enlarged [41]. The structures are grown mainly by MBE on semi-insulating GaAs substrate. These structures consist of a periodic array of Si-doped ($N_d \approx 10^{18}\,cm^{-3}$) GaAs quantum wells of thickness L_w separated by undoped $Al_xGa_{1-x}As$ barriers of thickness L_b. For operation at $\lambda = 7-11$ μm typically $L_w = 4$ nm, $L_b = 50$ nm, x = 0.25−0.30 and 50 periods are grown. The active structures are sandwiched between about 1 μm−thick heavily doped (also $N_d \approx 10^{18}$ cm^{-3}) GaAs contact layers. The photoconductive detectors are then fabricated by etching mesas through the superlattice. Ohmic contacts are made to the n^+-doped GaAs contact layers. To improve the optical coupling, the gratings are used. Usually, a 45° bevel is polished on one edge of the sample to facilitate optical measurements (see Fig. 5). The responsivity spectrum of GaAs/AlGaAs QW IR photoconductor shown in Fig. 6, has excellent peak responsivity of 1.2 A/W at bias voltage 3 V and $\lambda_p = 9.8$ μm and a long wavelength cutoff of $\lambda_c = 10.7$ μm. The detectivity of this photoconductor as a function of temperature and bias is shown in Fig. 7. The peak detectivity, for example, at 77 K and $V_b = 0.5$ V, is 6×10^9 $cmHz^{1/2}W^{-1}$, and 2×10^{10} $cmHz^{1/2}W^{-1}$ at 70 K. The first IR camera with such QW structure of 10 pixels GaAs array was demonstrated with high noise equivalent temperature difference sensitivity ($NE\Delta T < 0.1°C$) [42].

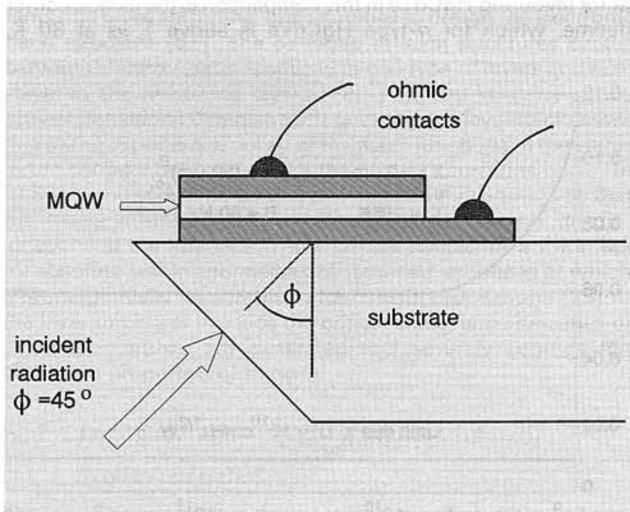

Fig. 5. GaAs/AlGaAs QWIP cross section (after Ref. [36])

The QW IR photodetectors have been also demonstrated using InP based materials system such as lattice matched GaAs/GaInP [43], InP/InGaAs [44], InP/InGaAsP [45] heterosystems. The responsivities of n-doped InP/InGaAs MQW IR photoconductors operating at wavelengths of $\lambda \approx 8$ μm were in fact somewhat larger than those obtained in equivalent GaAs/AlGaAs one. Recently long wavelength ($\lambda_c = 13.2$ μm) MQW detectors using lattice matched InP/InGaAsP material system and the first short wavelength ($\lambda_c = 2.7$ μm) photodetector in p-type InP/GaInAs material system were demonstrated too.

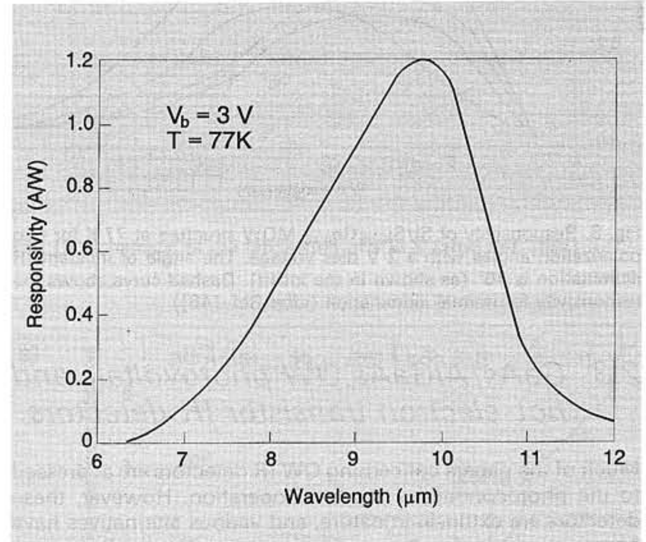

Fig. 6. Spectral dependence of responsivity for GaAs/AlGaAs QWIP at 77 K and $V_b = 3$ V (after Ref. [42])

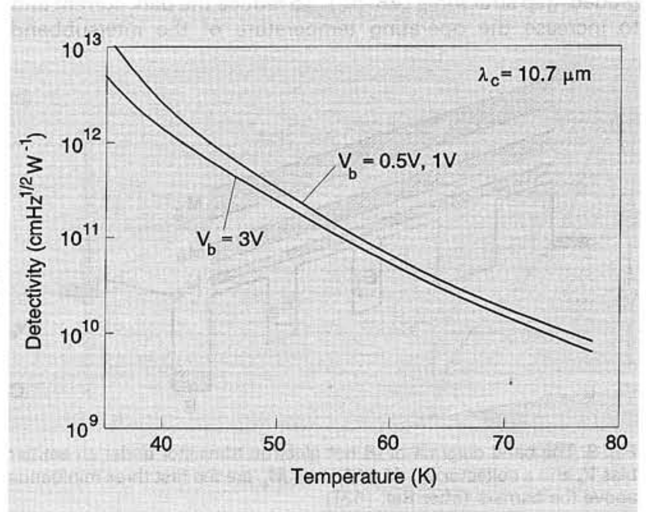

Fig. 7. Peak detectivity as a function of temperature and bias voltage for GaAs/AlGaAs QWIP (after Ref. [42])

2.2. $Si_{1-x}Ge_x/Si$ intersubband detectors

In SiGe/Si system for a $Si_{0.85}Ge_{0.15}$ QW with $L_w = 3$ nm, the optical absorption near 10 μm would be possible between the ground and extended state which is lying above the Si barrier [46]. The photoresponse of the SiGe/Si MQW IR detectors was observed at 77 K with a 2 V bias [47]. The responsivity and detectivity with peak near 7.5 μm were about 0.6 A/W and 10^9 cmHz$^{1/2}$W^{-1}, respectively. The normal incidence absorption demonstrated in SiGe/Si MQWs (see Fig. 8) indicates the possible realization of IR FPAs (field programmable arrays) without use the grating couplers normally required for GaAs/AlGaAs intersubband photodetectors. Detailed discussion of absorption mechanisms in SiGe/Si MQW structures may be found in Refs. [34,46].

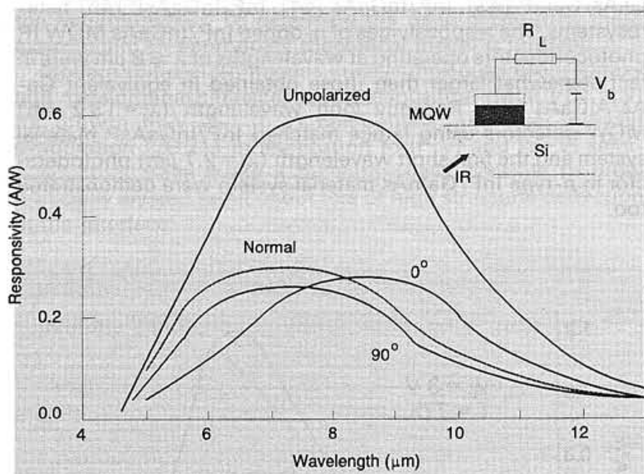

Fig. 8. Responsivity of $Si/Si_{0.85}Ge_{0.15}$ MQW structure at 77 K for two polarization angles with a 2 V bias voltage. The angle of incident IR illumination is 45° (as shown in the insert). Dashed curve shows the responsivity for normal illumination (after Ref. [46])

2.3. GaAs/AlGaAs QW photovoltaic and hot-electron transistor IR detectors

Much of the papers concerning QW IR detectors are addressed to the photoconductive mode of operation. However, these detectors are extrinsic in nature, and various alternatives have been suggested for future development. These alternatives include low-power and low-noise operation of MQW photovoltaic (PV) and hot-electron transistor detectors. Generally, photovoltaic effect is obtained in asymmetrical QWs including graded-gap structures [48–51]. To reduce the dark current and to increase the operating temperature of the intersubband detectors the IR hot-electron transistor was proposed [52,53]. The band diagram of IR hot-electron transistor is shown in Fig. 9. The performance of preliminary designed QW PV detectors are inferior in comparison with intersubband photoconductors. As for IR hot-electron transistor the improved one was grown on a (100) semi-insulating substrate [53] and the detectivity of the transistor increased up to $1.4 \cdot 10^{10}$ cmHz$^{1/2}$W^{-1} at 77 K with $\lambda_c = 9.5$ μm, that is two times larger as the companion state of the art GaAs MQW photoconductive detector.

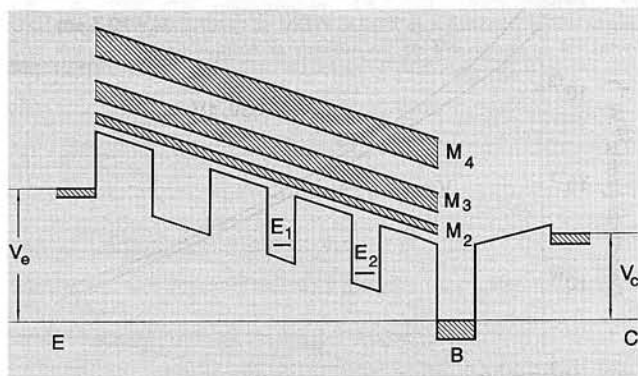

Fig. 9. The band diagram of IR hot electron transistor under an emitter bias V_e and a collector V_c. M_2, M_3, and M_4, are the first three minibands above the barriers (after Ref. [52])

Fig. 11. Plot of NEΔT at $\lambda = 10$ μm. The calculated curve assumes a $T_b = 295$ K, $A = 2500$ μm², $f/2$ optics, and $\Delta f = 60$ Hz (after Ref. [54]) ▶

2.4. Intersubband MQW IR detector arrays

In spite of achievement in GaAs/AlGaAs MQW IR detectors technology, direct bandgap intrinsic semiconductor, as typed

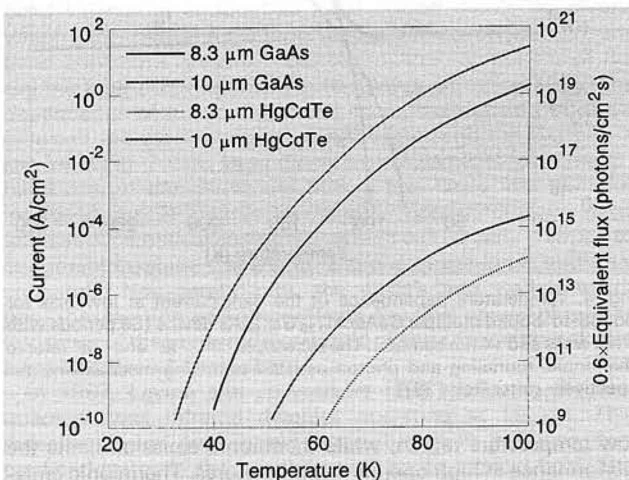

Fig. 10. Thermal generation current vs temperature for GaAs/AlGaAs QWIP and HgCdTe alloys at $\lambda_c = 8.3$ μm and 10 μm (after Ref. [55])

by HgCdTe, exhibit superior performance to the GaAs/AlGaAs superlattice at the same cut-off wavelength and temperature. Kinch and Yariv [54] have presented an investigation of the fundamental physical limitations of individual MQW IR detectors as compared to ideal HgCdTe detectors. Fig. 10 compares the thermal generation current versus temperature for GaAs/AlGaAs MQW SLs and HgCdTe alloys at $\lambda_c = 8.3$ μm and 10 μm. It is readily apparent from this figure that for HgCdTe the thermal generation rate at any specific temperature and cut-off wavelength is approximately five orders of magnitude smaller than for the corresponding GaAs/AlGaAs SL. The dominant factor favouring HgCdTe in this comparison is the excess carrier lifetime, which for n-type HgCdTe is above 1 μs at 80 K,

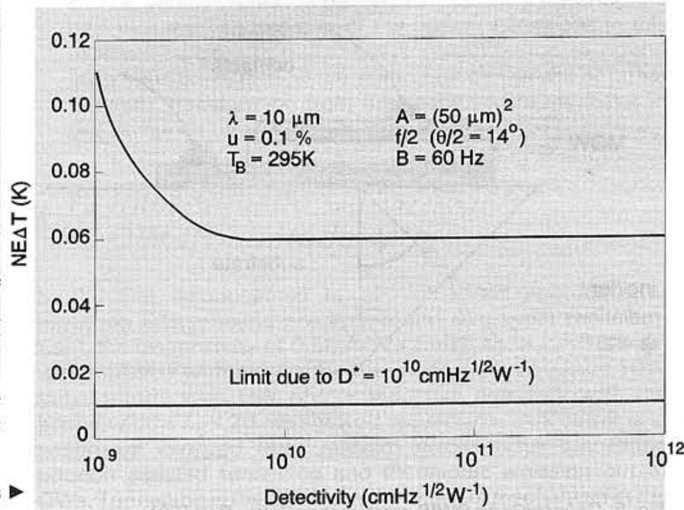

compared to 8.5 ps for the GaAs/AlGaAs SL. In SL the confined carriers are free to move within the plane (there is no energy gap separating confined from unconfined states), so the carrier recombination rate is very high. Plotted on the right-hand axis of Fig. 10 is the equivalent minimum temperature of operation in BLIP condition. For example, at a typical system background flux of 10^{16} photons/cm^{2}s, the required temperature of operation for the 8.3 μm (10 μm) GaAs/AlGaAs SL is below 69 K (58 K) to achieve the BLIP condition. In spite of the fact that performance of GaAs/AlGaAs intersubband MQW photodetectors are inferior in comparison with HgCdTe ones, these detectors with a $\lambda_c \approx 10$ μm and detectivity at 77 K can be used in many applications, especially in large two-dimensional FPAs. In contrast to HgCdTe, GaAs-based QW IR detector arrays promise high yield due to well established and highly uniform MBE growth and processing technologies for wafers of large square.

For large arrays the relevant figure of merit is the noise equivalent temperature difference ($NE\Delta T$), the temperature change of a scene required to produce a signal equal to the *rms* noise. An array having $D^* = 10^{10}$ cmHz$^{1/2}$W^{-1} would achieve a very sensitive $NE\Delta T = 0.01$ K (see Fig. 11). This would produce an excellent image, comparable or superior to that of present arrays which are uniformity limited. In this regard, it is worth noting, even for a highly uniform array having only a 0.1% pixel variation, that this small non-uniformity would limit $NE\Delta T$ to 0.06 K. Thus higher values of detectivity are unnecessary and in fact will not improve this limit as shown in Fig. 11.

Recently, the first hybrid 128x128 GaAs/AlGaAs MQW FPA's have been demonstrated [55, 56]. Levine et al. [55] have presented thermal imaging data a array of 50-μm square photoconductors having peak response at $\lambda_p = 9$ μm. To improve the optical coupling, the gratings were used. The arrays were bonded by Amber Engineering to their 128x128 InSb camera Si multiplexer. The 99% yield of this GaAs array technology is a result of the excellent MBE growth uniformity (1%) in thickness and the mature GaAs processing technology. After correction, measured non-uniformity of the array was better than 0.1%, and an $NE\Delta T$ of 0.01 K was observed at 60 K. It should be noticed that these array results are far from optimum. Implementing of improvements (structure of quantum wells, gratings, multiplexer, proper bias voltage) should improve the performance, raise the operation temperature to 77 K, and thus make GaAs SP's competitive and superior in array size, cost and yield to present HgCdTe arrays.

3. Interband type II IR SL photodetectors

GaAs/AlGaAs and some other III-V type I systems are very close lattice matched and so have rather perfect interface. Now it is also quite possible to grow high quality III-V type II SSLs for IR photoelectronics with the significantly different lattice constants that gives additional opportunities to design the electronic band structure [57]. The bandgap in such structures occurs between electron states localized in one type of layers and hole states in the remaining layers (Fig. 12). The intensity of the optical transitions diminish with growing the layer thicknesses due to the exponential decay of the wave functions of the states in the barriers, between which the optical transitions occur. In SLSs the individual material layers must be thin enough so that the lattice mismatch between the layers does generate dislocations at the interface. There are the critical layer thickness for absolute stable and metastable strained structures at which it is energetically favourable to form misfit dislocations [23]. If the layer thickness exceeds the critical value, large densities of misfit dislocations are generated that severely degrade the electronic properties of material.

3.1. $InSb/InAs_{1-x}Sb_x$ strained layer superlattices

The InAsSb ternary alloy does not have a sufficiently small gap suitable for operation in 8–14 μm atmospheric window at 77 K, but recently work has intensively begun on III-V mismatched

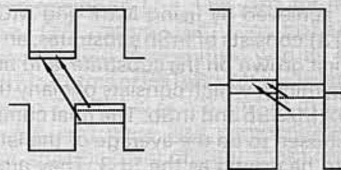

Fig. 12. Type II band offsets which can produce band-to-band transition energies less than the bulk bandgap energies of the materials. The broken lines represent the resulting energy levels (after Ref. [63])

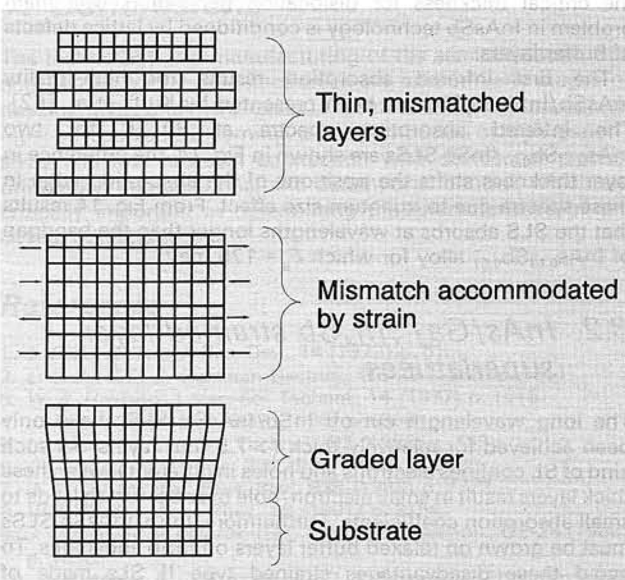

Fig. 13. Schematic of the fabrication of a SLS (after Ref. [58])

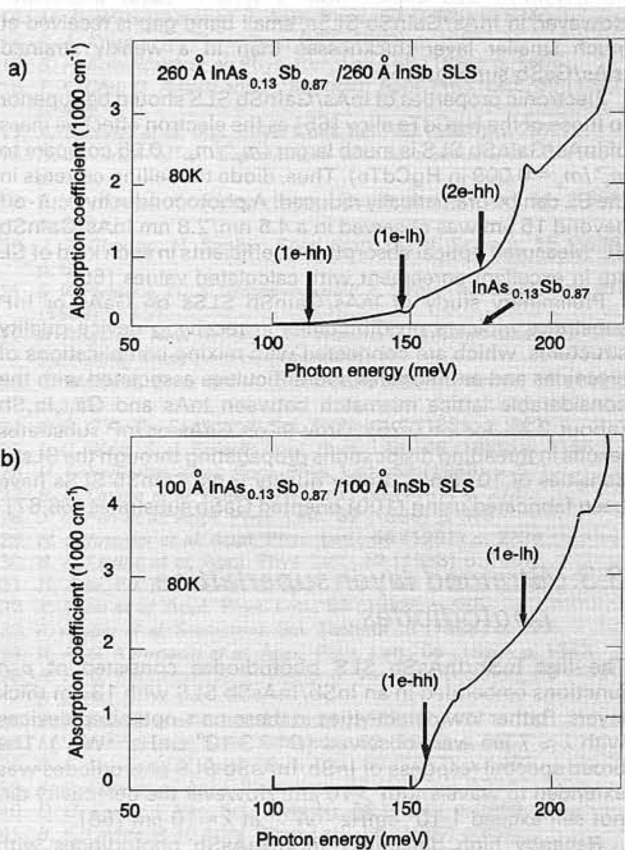

Fig. 14. Infrared absorption spectra of $InAs_{0.13}Sb_{0.87}$/InSb SLSs with 26 nm thick layers (a) and 10 nm thick layer (b) (after Ref. [62])

SLS systems [58-61]. A serious step InAsSb SLSs development has been achieved by using MBE and MOCVD. Typical structure (Fig. 13) consists of InSb substrates, an InAsSb buffer layer which is first grown on the substrate, and finally superlattice (about 1 μm thick), which consists of many thin alternating strained layers of InAsSb and InSb. The final composition of the buffer layer is chosen to be the average of the lattice constants of alloy layers to be grown as the SLS. They are shown in the upper part of the Fig. 13 in their unstrained form. All of the lattice mismatch is accommodated by strain in each thin SLS layer (tensile in one, compression in other) without the generation of misfit dislocation if the individual layers are below the critical thickness for dislocation generation. The main problem in InAsSb technology is conditioned by lattice defects of buffer layers.

The first infrared absorption results for high-quality InAsSb/InSb SLSs have been presented by Kurtz et al. [62]. The infrared absorption spectra at 80 K for two $InAs_{0.13}Sb_{0.87}$/InSb SLSs are shown in Fig. 14. the difference in layer thickness shifts the positions of the absorption edge in these spectra due to quantum size effect. From Fig. 14 results that the SLS absorbs at wavelengths longer than the bandgap of $InAs_{0.13}Sb_{0.87}$ alloy for which $E_g = 175$ meV.

3.2. $InAs/Ga_{1-x}In_xSb$ strained layer superlattices

The long wavelength cut-off InSb/InAsSb SLSs have only been achieved for relatively thick (>7.5 nm) layers. As such kind of SL confines electrons and holes in different layers, these thick layers result in small electron-hole overlap, which leads to small absorption coefficients. Furthermore, InSb/InAsSb SLSs must be grown on relaxed buffer layers on InSb substrates. To avoid these disadvantages strained type II SLs made of InAs/GaInSb have been proposed as a new material system for IR detectors [23,65]. Like InSb/InAsSb system, IR response in InAs/GaInSb SLs comes from a type II band alignment. However, in InAs/GaInSb SLSs, small band gap is received at much smaller layer thicknesses than in a weakly strained InAs/GaSb superlattice.

Electronic properties of InAs/GaInSb SLS should be superior to those of the HgCdTe alloy [65] as the electron effective mass of InAs/GaInSb SLS is much larger ($m_e^*/m_o = 0.05$ compare to $m_e^*/m_o = 0.009$ in HgCdTe). Thus, diode tunnelling currents in the SL can be dramatically reduced. A photoconductive cut-off beyond 15 μm was observed in a 4.5 nm/2.8 nm InAs/GaInSb SL. Measured optical absorption coefficients in such kind of SL are in excellent agreement with calculated values [66].

Preliminary study of InAs/GaInSb SLSs on GaAs or InP substrates indicate on difficulties in receiving device-quality structures, which are connected with mixing complications of arsenides and antimonides and difficulties associated with the considerable lattice mismatch between InAs and $Ga_{1-x}In_xSb$ (about 2.2% for $x = 0.25$). Growth on GaAs or InP substrates results in threading dislocations propagating through the SLs in densities of 10^9 cm^{-2}. Better quality InAs/GaInSb SLSs have been fabricated using (100) oriented GaSb substrates [66,67].

3.3. Strained layer superlattice photodiodes

The first InSb/InAsSb SLS photodiodes consisted of *p-n* junctions embedded in an InSb/InAsSb SLS with 13 nm thick layers. Rather low detectivities in these non-optimized devices with $\lambda \approx 7$ μm were observed ($D^* = 3 \cdot 10^9$ cmHz$^{1/2}$W^{-1}). The broad spectral response of InSb/InAsSb SLS photodiodes was extended to wavelength >10 μm. However the detectivity did not still exceed $1 \cdot 10^9$ cmHz$^{1/2}$W^{-1} at $\lambda = 10$ μm [68].

Recently high detectivity InSb/InAsSb photodiodes with $D^* > 10^{10}$ cmHz^{1}/W^{-1} at $\lambda < 10$ μm were fabricated [69]. The structure and composition of the InAsSb SLS photodiode is shown in Fig. 15. The SLS was grown on top of thick,

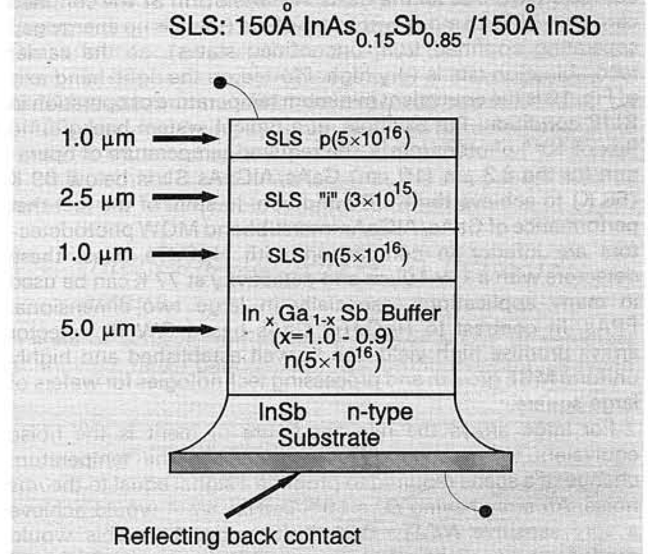

Fig. 15. Structure and composition of the InAsSb SLS photodiode (after Ref. [63])

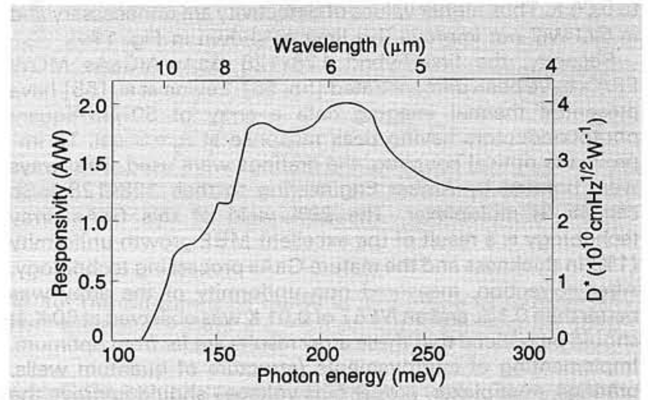

Fig. 16. Responsivity and detectivity of $InAs_{0.15}Sb_{0.85}$/InSb SLS photodiode at 77 K (after Ref. [64])

composition-graded InGaSb strain-relief buffer on an InSb substrate. The photodiode *p-i-n* structure was embedded in the superlattice with 15 nm thick layers. The resistance-area product (R_oA) equal to 9 Ωcm^2 was achieved at 77 K after a crude passivation. The temperature dependence of the R_oA product indicates that performance of detector is not yet limited by diffusion or depletion region generation-recombination processes. The Fig. 16 shows the zero-bias current responsivity and detectivity for InAsSb/InSb photodiode.

To date, growth of above structures on InSb substrates, which places the SLS under net tension, usually leads to cracking of the epitaxial material, precluding the fabrication of detector arrays. The growth of similar structures on GaSb and InAs substrates, which places the SLS in net compression, eliminates the cracking problem, but requires a much large mismatch between SLS and substrate. A key factor in the successful growth of these structures is the use of the InAlSb/AlSb SLS as a digital buffer [70].

The possibility of fabrication of *p-n* junctions also in InAs/GaInSb SLS system has been recently demonstrated too [66]. The spectral response of 2.4nm/4.0nm InAs/GaInSb backside-illuminated SLS photodiode had a threshold near 12 μm.

Above presented results concerning SLS photodiodes performance are encouraging. However, one can not presently claim that these structures in near future will replace HgCdTe. Progress in their development depends on continued improvements in material growth, device processing, and understanding of SLS electronic properties.

4. HgTe/CdTe and related superlattices

HgTe/CdTe SLs belong to type III SLs. Type III to type I transition in HgCdTe/CdTe and related SLs (e.g. HgZnTe/CdTe, HgMnTe/CdTe) was observed experimentaly [71,72].

HgTe/CdTe system was the first from a new class of structures for IR optoelectronics, which has received a great deal of attention since 1979, when this SL system was proposed [73]. To date however, attempts to realize HgTe/CdTe and related SLs with properties suitable for IR detection are unsuccessful. It seems to be determined by interface instabilities of SLs due to weak Hg chemical bonding in the material leading to large Hg diffusion coefficients even at rather moderate temperatures [72,73], as well as by basic problems associated with the SL's band structure leading to the necessity of producing thin (<5.0 nm) constituent layers and thus closely connected with the first problem.

The valence band offset between HgTe and CdTe has a crucial influence on the HgTe/CdTe SL band structure. Recently there have been obtained evidences [76,77] of large valence band offset ($\Delta E_v \approx 350$ meV) in HgTe/CdTe SLs which is temperature independent. *In situ* XPS experiments [72] have shown that the valence-band offset is independent of the surface (100), (110) and (111)B orientation.

In spite of failure of HgTe/CdTe SLs IR optoelectronics applications, the studies of these SLs are intensively continued (e.g. Ref. [78]) considering their unique physical properties.

5. Doping superlattices

The electrons and holes in doping SLs are spatially separated that leads, first of all, to an excess carrier recombination lifetime, which can be larger by many orders of magnitude than those in the host material. So far, nearly all of the experimental investigations and most of the theoretical studies on doping SLs, have dealt with GaAs doping SL structures (called also "*n-i-p-i* structures"). The doping SLs were pursued especially by Ploog and Dohler in their two comprehensive reviews [79,80]. The *n-i-p-i* SL concept has been known for several years but only recently this concept was demonstrated in application to mid-and long-wavelength IR photodetectors.

The most promising for long wavelength IR detectors fabrication are *n-i-p-i* structures from InSb and InAs [81,82] although encouraging results were obtained with PbTe *n-i-p-i* structures [83].

6. IV–VI superlattices and quantum well structures

IV–VI semiconductors are mainly used in applications to 2–15 μm IR detectors and as well as IR diode lasers for the region of wavelengths $\lambda \approx 3-45$ μm. IV–VI laser diodes are mainly used in spectroscopic applications. Only IV–VI SLs and QWs today form a real alternative for these applications in IR region as with narrowing band gap the stimulated emission is a dominating process of recombination in these structures in contrast, e.g., to HgCdTe-like narrow gap alloys and structures. The reason of it lies in a higher density of states and lower Fermi energies for the same injected carrier densities in IV–VI structures compare to II–VI or III–V materials and structures. This enhances the radiative recombination rate compare to the Auger one.

The advantages of IV–VI QW and SL structures for IR laser applications are induced by the fact that the population inversion in QW structures is more easily be obtained due to:

a) step-like density of states and effective carrier confinement,
b) appropriate doping of the constituents,
c) more effective mode control.

These are the reasons for more effective operation even at elevated temperatures compare to diode lasers, as much lower threshold currents can be achieved [84,85].

The current state-of-the-art for maximum operating temperatures of QW IV-VI lasers enable to elevate the temperature of CW laser operation up to 174 K ($\lambda = 4.39$ μm) and up to 270 K for pulsed operation ($\lambda = 3.88$ μm) for lattice matched PbTe/PbEuTeSe QW lasers [86]. In PbSe/PbEuSe QW diode laser the operating temperature was as high as 220 K ($\mu = 4.4$ μm) [87]. PbSnTe/PbTeSe MQW lasers operating in pulsed mode up to $T = 204$ K ($\lambda = 6$ μm) or in CW mode up to $T = 130$ K ($\mu = 6.6$ μm) were also demonstrated [84]. Thus, from application-specific point of view, these results mean that relatively simple and inexpensive cooling systems based on the Peltier or Joule-Thomson effect may be used at least for mid-IR IV-VI QW lasers.

7. Conclusions

The technology and manufacturing of the semiconductor SLs and MQWs for IR optoelectronics are now in early stages of development, and here exsist a number of questions which must be resolved concerning, e.g.: optimization of high responsivity and low noise in connection with device parameters, uniformity, compositional and dimentional control; which are critically important in determining the characteristics of the device operation.

References

1. *L. Esaki, R. Tsu:* J. Res. Dev., **14** (1970) p. 61.
2. *L. Esaki:* IEEE J. Quantum Electron., **QE-22** (1986) p. 1611.
3. *W. A. Harrison:* J. Vac. Sci. Technol., **14** (1977) p. 1016.
4. *J. Tersoff:* Phys. Rev., **B32** (1985) p. 6968.
5. *H. Kromer:* J. Vac. Sci. Technol., **B2** (1988) p. 433.
6. *G. Margaritondo:* Phys. Rev., **B31** (1985) p. 2526.
7. *J. M. Langer et al:* Phys. Rev., **B38** (1988) p. 7723.
8. *W. Pollard:* J. Appl. Phys., **69** (1991) p. 3154.
9. *J. Menendez, A. Pinczuk:* IEEE J. Quantum Electron., **QE-24** (1988) p. 1698.
10. *R. C. Miller, A. C. Gossard and D. A. Kleinmann:* Phys. Rev., **B32** (1985) p. 5443.
11. *K. Yamanaka et al:* Appl. Phys. Lett., **48** (1986) p. 840.
12. *H. Okimura et al:* Appl. Phys. Lett., **46** (1985) p. 377.
13. *M. O. Watanabe et al:* J. Appl. Phys., **57** (1985) p. 5340.
14. *E. A. Kraut et al:* Phys. Rev., **B27** (1983) p. 1965.
15. *S. P. Kowalczyk et al:* Phys. Rev. Lett., **56** (1986) p. 1605.
16. *T. K. Chu, D. Agassi and A. Martinez:* Appl. Phys. Lett., **50** (1987) p. 419.
17. *A. Lechner et al:* Inst. Phys. Conf. Ser., **83** (1986) p. 267.
18. *H. Heinrich et al:* Superlattices and Microstructures, **5** (1989) p. 175.
19. *E. O. Gobel, K. Ploog:* Progr. Quantum Electron., **14** (1991) p. 289.
20. *J. T. Cheung, H. Sankur:* Solid State Mater. Science, **15** (1988) p. 63.
21. *S. V. Plyatsko, Yu. S. Gromovoj and F. F. Sizov:* Thin Solid Films, **218** (1992) p. 151.
22. *A. Rogalski:* New ternary alloy systems for infrared detectors. SPIE Publishing Press (will be published).
23. *C. Mailhiot, D. L. Smith:* Solid State Mater. Science, **16** (1990) p. 131.
24. *E. P. O'Reilly:* Semicond. Sci. Technol., **4** (1989) p. 121.
25. *L. C. West, S. J. Eglash:* Appl. Phys. Lett., **46** (1985) p. 1156.
26. *H. Lobentanzer et al:* Appl. Phys. Lett., **53** (1988) p. 571.
27. *B. F. Levine et al:* Appl. Phys. Lett., **50** (1987) p. 273.
28. *J. L. Pan et al:* Appl. Phys. Lett., **57** (1990) p. 366.
29. *H. Schneider et al:* Appl. Phys. Lett., **58** (1991) p. 2234.
30. *B. F. Levine et al:* Appl. Phys. Lett., **52** (1988) p. 1481.
31. *H. Asai, Yu. Kawamura:* J. Appl. Phys., **68** (1990) p. 5890.
32. *X. Zhou et al:* Appl. Phys. Lett., **54** (1989) p. 855.
33. *F. Muller et al:* Semicond. Sci. Technol., **3** (1988) p. 797.
34. *R. P. G. Karunasiri et al:* Appl. Phys. Lett., **56** (1990) p. 1342.
35. *R. P. G. Karunasiri, K. L. Wang:* J. Vac. Sci. Technol., **B9** (1991) p. 2064.
36. *B. F. Levine et al:* Electr. Lett., **24** (1988) p. 747.
37. *M. Zaluzny:* Solid State. Commun., **82** (1992) p. 565.
38. *B. F. Levine et al:* Appl. Phys. Lett., **50** (1987) p. 1092.
39. *K. K. Choi et al:* Appl. Phys. Lett., **50** (1987) p. 1814.
40. *D. D. Coon:* J. Vac. Sci. Technol., **A8** (1990) p. 2950.
41. *B. F. Levine et al:* Appl. Phys. Lett., **56** (1990) p.851.
42. *C. G. Bethea et al:* IEEE Trans. Electron. Devices, **38** (1991) p. 1118.
43. *S. D. Gunapala et al:* Appl. Pys. Lett., **57** (1990) p. 1802.

44. *S. D. Gunapala et al:* Appl. Phys. Lett., **58** (1991) p. 2024.
45. *S. D. Gunapala et al:* Proc. SPIE, **1541** (1991) p. 11.
46. *R. P. G. Karunasiri, J. S. Park and K. L. Wang:* Appl. Phys. Lett., 59 (1991) p. 2588.
47. *J. S. Park, R. P. G. Karunasiri and K. L. Wang:* Appl. Phys. Lett., 60 (1992) p. 103.
48. *A. Kastalsky et al:* Appl. Phys. Lett., 52 (1988) p. 1320.
49. *K. W. Goossen, S. A. Lyon:* J. Appl. Phys., 63 (1988) p. 5149.
50. *S. A. Lyon:* Surf. Sci, 228 (1990) p. 508.
51. *D. D. Coon et al:* J. Vac. Sci. Technol., A9 (1991) p. 863.
52. *K. K. Choi et al:* Appl. Phys. Lett., **57** (1990) p. 1348.
53. *K. K. Choi et al:* Appl. Phys. Lett., **59** (1991) p. 3303.
54. *M. A. Kinch, A. Yariv:* Appl. Phys. Lett., **55** (1989) p. 2093.
55. *B. F. Levine et al:* Semicond. Sci. Technol., 6 (1991) p. C114.
56. *L. J. Kozlowski et al:* IEEE Trans. Electron. Devices, 38 (1991) p. 1124.
57. *G. C. Osbourn:* J. Vac. Sci. Technol., B2 (1984) p. 176.
58. *G. C. Osbourn:* IEEE J. Quantum Electron., **QE-22** (1986) p. 1677.
59. *L. R. Dawson:* J. Cryst. Growth, **98** (1989) p. 220.
60. *R. A. Stradling:* Proc. SPIE, **1361** (1990) p. 630.
61. *R. M. Biefeld, J. R. Wendt and S. R. Kurtz:* J. Crystal Growth, **107** (1991) p. 836.
62. *S. R. Kurtz et al:* Appl. Phys. Lett., **53** (1988) p. 1961.
63. *G. C. Osborn:* Semicon. Sci. Technol., 5 (1990) p. S5.
64. *S. R. Kurtz et al:* IEEE Electr. Device Lett., 11 (1990) p. 54.
65. *C. Mailhiot, D. L. Smith:* J. Vac. Sci. Technol., **A7** (1989) p. 445.
66. *D. H. Chow et al:* Semicond. Sci. Technol., 6 (1991) p. C47.
67. *R. H. Miles, D. H. Chow and W. J. Hamilton:* J. Appl. Phys., **71** (1992) p. 211.
68. *S. R. Kurtz et al:* Proc. SPIE, **930** (1988) p. 101.
69. *S. R. Kurtz et al:* IEEE Electr. Dev. Lett., **10** (1989) p. 150.
70. *L. R. Dawson:* private information.
71. *J. P. Faurie et al:* J. Vac. Sci. Technol., B5 (1987) p. 700.
72. *X. Chu, S. Sivananthan and J. P. Faurie:* Superlattices and Microstructures, **4** (1988) p. 173.
73. *J. N. Schulman, T. C. McGill:* Appl. Phys. Lett., **34** (1979) p. 663.
74. *J. L. Staudenmann, R. D. Knox and R. D. Horning:* J. Cryst. Growth., 86 (1988) p. 436.
75. *K. K. Mahavadi et al:* Appl. Phys. Lett., **56** (1990) p. 2077.
76. *S. P. Kowalczyk et al:* Phys. Rev. Lett., 56 (1986) p. 1605.
77. *C. R. Becker et al:* Semicond. Sci. Technol., **6** (1991) p. C76.
78. *J. R. Meyer, C. A. Hoffman and R. J. Bartoli:* Semicond. Sci. Technol., **5** (1990) p. S90
79. *K. Ploog, G. H. Dohler:* Advances in Physics, 32 (1983) p. 285.
80. *G. H. Dohler:* Optical and Quantum Electronics, 22 (1990) p. 121.
81. *J. Maserjian, F. J. Grunthaner and C. T. Elliott:* Infrared Phys., **30** (1990) p. 27.
82. *C. C. Phillips:* Appl. Phys. Lett., **56** (1990) p. 151.
83. *G. Bauer, W. Jantsch:* Proc. SPIE, **943** (1988) p. 107.
84. *K. Shinohara et al:* Appl. Phys. Lett., **47** (1985) p. 1184.
85. *D. L. Partin:* IEEE J. Quantum Electron., 24 (1988) p. 1716.
86. *D. L. Partin:* Superlattices and Microstructures, **1** (1985) p. 131.
87. *R. Rosma et al:* IEEE J. Quantum Electron., **QE-23** (1987) p. 94.